# Architecture of the high mobility group nucleosomal protein 2-nucleosome complex as revealed by methyl-based NMR

Hidenori Kato[a,1], Hugo van Ingen[b,1], Bing-Rui Zhou[a,1], Hanqiao Feng[a], Michael Bustin[c], Lewis E. Kay[b], and Yawen Bai[a,2]

[a]Laboratory of Biochemistry and Molecular Biology, Center for Cancer Research, National Cancer Institute, National Institutes of Health, Bethesda, MD 20892; [b]Departments of Molecular Genetics, Biochemistry, and Chemistry, University of Toronto, Toronto, ON, Canada M5S 1A8; [c]Laboratory of Metabolism, Center for Cancer Research, National Cancer Institute, National Institutes of Health, Bethesda, MD 20892

Edited by Adriaan Bax, National Institutes of Health, Bethesda, MD, and approved May 31, 2011 (received for review April 13, 2011)

**Chromatin structure and function are regulated by numerous proteins through specific binding to nucleosomes. The structural basis of many of these interactions is unknown, as in the case of the high mobility group nucleosomal (HMGN) protein family that regulates various chromatin functions, including transcription. Here, we report the architecture of the HMGN2-nucleosome complex determined by a combination of methyl-transverse relaxation optimized nuclear magnetic resonance spectroscopy (methyl-TROSY) and mutational analysis. We found that HMGN2 binds to both the acidic patch in the H2A-H2B dimer and to nucleosomal DNA near the entry/exit point, "stapling" the histone core and the DNA. These results provide insight into how HMGNs regulate chromatin structure through interfering with the binding of linker histone H1 to the nucleosome as well as a structural basis of how phosphorylation induces dissociation of HMGNs from chromatin during mitosis. Importantly, our approach is generally applicable to the study of nucleosome-binding interactions in chromatin.**

Packaging of the eukaryotic genome into chromatin is regulated by numerous chromatin factors and enzymes that bind to nucleosomes (1–4), the fundamental building block of chromatin that is formed by approximately 146 base pairs of DNA wrapped around an octamer containing two copies each of histone H2A, H2B, H3, and H4 (Fig. 1 *A* and *B*) (5–7). Despite the central role of these interactions in chromatin biology and gene regulation, little structural information is available on how chromatin enzymes and factors recognize nucleosomes, in particular for those recognitions that are independent of post-translational modifications of histone tails. High mobility group nucleosomal (HMGN) proteins are a family of such proteins that exist in vertebrate. HMGNs decompact chromatin condensed by the linker histone H1 (8), thereby enhancing transcription activity of the chromatin template. In addition, HMGNs affect DNA repair (9), chromatin remodeling (10), and the extent of histone modifications (11).

The function of HMGNs depends on their ability to bind two high affinity sites on the nucleosome (12), using a conserved nucleosome-binding domain (NBD) (9, 12, 13). Elucidation of the structural basis of this interaction has proven to be challenging because HMGNs are intrinsically disordered and their nucleosome-binding domains interact with the nucleosome core (Fig. S1) (13), precluding the use of histone peptide models (14). Attempts to grow crystals of the HMGN2-nucleosome complex were so far unsuccessful. In general, it is difficult to obtain diffraction quality crystals of proteins complexed with nucleosomes (4). Up to date, only two structures of protein–nucleosome complexes have been determined using X-ray crystallography (15, 16), even though many structures of nucleosome core particles containing histones from various species with either the human α-satellite or Widom's "601" DNA are available (4).

Here, we use solution NMR as our main tool to obtain structural information on the HMGN2-nucleosome complex. Because of its large size (approximately 230 kiloDaltons), we rely on recently developed the $^{1}H$-$^{13}C$ methyl-transverse relaxation optimized nuclear magnetic resonance spectroscopy (methyl-TROSY) method for macromolecules (17–19) to monitor the histone methyl groups in Ile, Leu, and Val (ILV) residues in the nucleosome and to identify HMGN2 binding sites on the nucleosome surface. In addition, we use mutational analysis to independently verify the results obtained by methyl-TROSY NMR. We find that HMGN2 staples the core histones and DNA by binding to the acidic patch on the H2A/H2B dimer and the DNA near the entry/exit point. We propose and verify a mechanism whereby the C-terminal region of HMGN2 interferes with the binding of linker histone H1 to the nucleosome. These studies show that our approach is capable of obtaining sufficient structural information to provide mechanistic insights into HMGNs function in a manner complementary to X-ray crystallography and opens the exciting possibility of structural studies of a range of different complexes involving the nucleosome core particle and binding targets.

## Results

**Chemical Shift Assignment of the Methyl Groups in the Nucleosome.** To assign the chemical shifts of the methyl groups in the nucleosome, we reconstituted the nucleosome with ILV-labeled and otherwise per-deuterated *Drosophila* histones and protonated Widom's 601 DNA (20). As in other NMR studies of supramolecular systems (18, 19), methyl-TROSY spectra of the nucleosome are of excellent quality (Fig. 1*C*). We obtained assignments for 89% of the histone ILV methyl groups (151 out of 170) through the combined analysis of 58 single mutations and a series of NOESY spectra, taking advantage of the crystal structure of the nucleosome [Protein Data Bank (PDB) ID code 2PYO] (Table S1, Table S2, and Fig. S2). Nearly all methyl groups are observed, displaying single cross-peaks reflecting the global twofold structural symmetry of the nucleosome. Notably, because the 601 DNA lacks sequence symmetry, a few methyl groups that are very close to local asymmetric sites on the DNA show split cross-peaks, one for each distinct site (Fig. S2) (7, 16). Additionally, methyl groups close to the protonated DNA have attenuated peak intensities, as the presence of external protons increases methyl group transverse relaxation rates.

**Identification of the HMGN2 Binding Sites on the Nucleosome.** With the assignment of the methyl groups, we then used chemical shift perturbation (CSP) to identify the nucleosome-binding sites of

Author contributions: H.K., H.v.I., B.-R.Z., H.F., L.E.K., and Y.B. designed research; H.K., H.v.I., B.-R.Z., and H.F. performed research; H.K., H.v.I., B.-R.Z., H.F., L.E.K., and Y.B. analyzed data; and H.v.I., M.B., L.E.K., and Y.B. wrote the paper.

The authors declare no conflict of interest.

This article is a PNAS Direct Submission.

See Commentary on page 12189.

[1]H.K., H.v.I., and B.-R.Z. contributed equally to this work.

[2]To whom correspondence should be addressed. E-mail: yawen@helix.nih.gov.

This article contains supporting information online at www.pnas.org/lookup/suppl/doi:10.1073/pnas.1105848108/-/DCSupplemental.

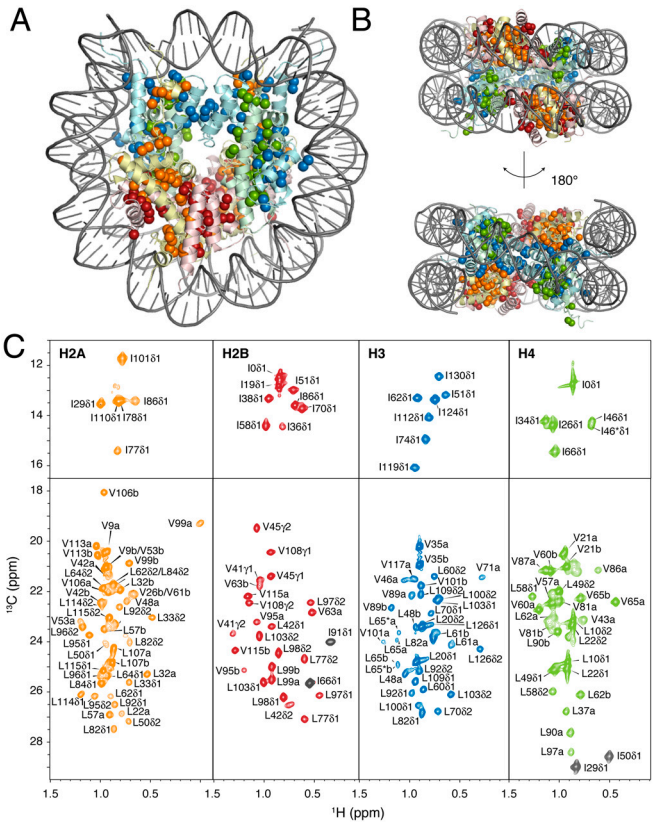


**Fig. 1.** *Structure and NMR spectra of the nucleosome.* (*A* and *B*) Distribution of assigned ILV methyl groups in the nucleosome (PDB ID code 2PYO) showing top (*A*) and side views (*B*). The backbone of the histones is shown with ribbons, ILV methyl groups as spheres. Color coding: H2A, orange; H2B, red; H3, blue; H4, green; DNA, gray. (*C*) Methyl-TROSY spectra of ILV methyl-labeled H2A, H2B, H3, and H4 in the nucleosome. (*Top*) The δ1 methyl groups of Ile residues. (*Bottom*) The Leu-δ1/δ2 and Val-γ1/γ2 methyl groups. Leu/Val methyl groups are labeled with their stereospecific assignments where available; otherwise the two methyl groups are arbitrarily assigned as "a" or "b." Aliased Ile-δ1 resonances are shown in gray. Ile0 represents the Ile inserted after the N-terminal Met for improving the yield of protein expression.

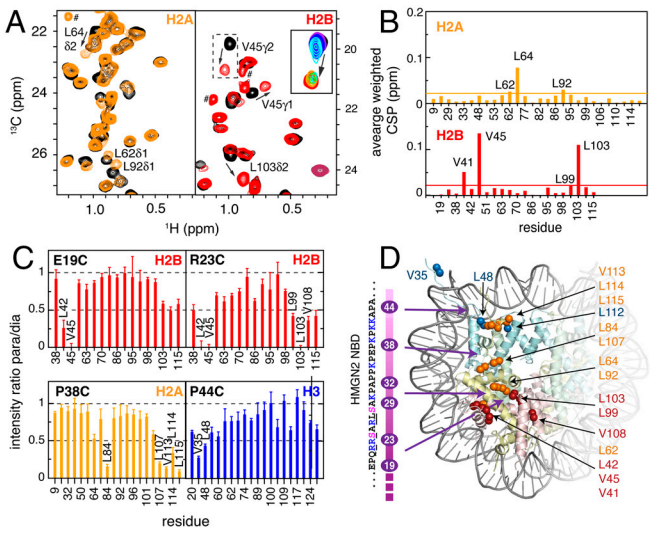


**Fig. 2.** *Identification of the interactions between HMGN2 and the nucleosome by chemical shift perturbation and paramagnetic spin labeling.* (*A*) Overlay of the spectra of free (black) and HMGN2-bound (orange or red) nucleosomes, reconstituted with either ILV-labeled H2A (*Left*) or H2B (*Right*). Methyl groups with significant chemical shift changes are labeled. (*Inset*) An overlay of several titration spectra for Val45γ2 in H2B. Resonances labeled with # are natural abundance signals from the disordered regions of HMGN2. (*B*) Chemical shift perturbation between free and bound states for H2A (*Top*) and H2B (*Bottom*). Residues with averaged, weighted CSP larger than the 10% trimmed mean + 2 SD are labeled. To identity the binding site of HMGN2, the average, weighted CSP of the histone ILV residues was calculated according to $\mathrm{CSP} = (1/N)\sum[(\Delta\delta^2_{\mathrm{H},i} + (\Delta\delta^2_{^{13}\mathrm{C},i} \times w_i)_2]^{1/2}$, where $\Delta\delta_i$ is the difference in peak position between the free and bound states in ppm for atom $i (i \in \{\mathrm{C}\gamma1/2, \mathrm{C}\delta1/2, \mathrm{H}\gamma1/2, \mathrm{H}\delta1/2\})$, the $^{13}$C chemical shift weighting factor $w_i$ is set $\sigma_{\mathrm{H},i}/\sigma_{\mathrm{C},i}$ (~0.16–0.18), $\sigma_i$ is the standard deviation of deposited chemical shifts in the Biological Magnetic Resonance Data Bank (41) for atom *i*, and the summation extends over the *N* methyl groups of each residue (i.e., $N = 1$ for Ile, and $N = 2$ for Leu/Val). (*C*) Methyl group peak intensity ratios, $I(Mn^{2+})/I(Ca^{2+})$, of paramagnetic $Mn^{2+}$-EDTA and diamagnetic $Ca^{2+}$-EDTA spin-labeled HMGN2 at positions 19, 23, 38 and 44. Intensity ratios of the two individual methyl groups for Leu/Val were averaged. Errors (1 SD) are denoted by thin bars. Residues with average intensity ratio+ 2 SD < 0.5 are labeled. (*D*), Structural summary of NMR CSP and paramagnetic spin labeling. Methyl groups with large chemical shift changes or decreases in peak intensity are labeled. Color coding as in Fig. 1. The sequence of the nucleosome-binding domain of HMGN2 and the position of the spin labels are shown (*Left*). Arg/Lys residues are highlighted in blue, and Ser24 and Ser28 are shown in magenta.

HMGN2. Upon binding of HMGN2 to the nucleosome, methyl groups Leu64δ2 in H2A and Val45γ2/Leu103δ2 in H2B displayed large chemical shift changes (Fig. 2 *A*, *B*, and *D*), whereas the methyl groups in histones H3 and H4 showed negligible changes (Fig. S3). The close spatial proximity of these three methyl groups to HMGN2 could be confirmed using a saturation transfer experiment that showed selective transfer of saturation of the HMGN2 proton magnetization to Val45γ2 and Leu103δ2 in H2B (Fig. S3). Moreover, we found that the N-terminal region (residues 19–30) of the NBD affects the same methyl groups in an isolated H2A-H2B dimer (Fig. S3). Interestingly, these methyl groups are very close to several negatively charged residues (Glu60, Glu63, Asp89, Glu90, Glu91 in H2A and Glu102 in H2B) (acidic patch) on the H2A/H2B dimer surface.

We next performed paramagnetic relaxation enhancement (PRE) experiments to obtain long-range distance information on the HMGN2-nucleosome complex (Fig. 2 *C* and *D* and Fig. S4). In the PRE experiments, each of the residues Glu19, Arg23, Ala29, Ala32, Pro38, and Pro44 in HMGN2 was mutated to Cys individually and linked by a disulfide bond to the paramagnetic compound S-Methanethiosulfonylcysteaminyl (MTS)-EDTA-$Mn^{2+}$. Binding of paramagnetic spin-labeled HMGN2 reduces peak intensities of the methyl groups in the nucleosome in a manner depending on their distances to the paramagnetic center (21). The N-terminal spin labels (Glu19, Arg23, Ala29, and Ala32) all affect methyl groups near the acidic patch, confirming the chemical shift perturbation results. Importantly, spin labels at positions Pro38 and Pro44 in HMGN2 affect methyl groups in the C-terminal part of H2A and the N-terminal part of H3 (Fig. 2 *C* and *D*), indicating that the C-terminal region of the binding domain is close to the region where the DNA enters/exits the nucleosome.

The binding sites identified by the methyl-TROSY studies were further verified by independently examining the effect of mutations in either HMGN2 or in the nucleosome using isothermal titration calorimetry (ITC). The single charge reversal mutation Glu60Lys or Glu63Lys or a neutralizing triple mutation Asp89-Ser/Glu90Thr/Glu91Thr in H2A abolishes binding of HMGN2, showing that the acidic patch is involved in the binding. Additionally, reduced binding affinity upon mutation of Glu102 to Thr in H2B supports its involvement in the interaction (Fig. 3 *A* and *B*). Conversely, mutation of either Arg22 or Arg26 to Ala in the NBD abolishes HMGN2 binding to the nucleosome (Fig. 3 *A* and *B*) (22). Binding of HMGN2 to DNA is apparent from the positive postbinding baseline that disappears upon simultaneous mutation of Lys35, Lys39, Lys41, and Lys42 in the NBD to

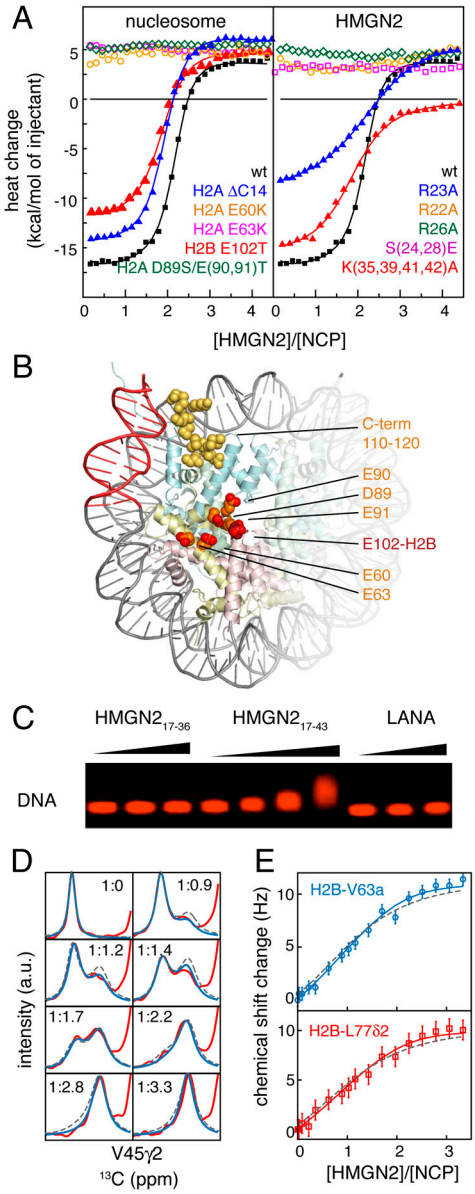


**Fig. 3.** *Binding of HMGN2 to the nucleosome (NCP) by mutation and NMR line-shape analysis.* (*A*) ITC titration results for wild-type HMGN2 with wild-type nucleosome (black) and selected mutants (20 mM Tris-HCl, 50 mM NaCl, 1 mM EDTA, 1 mM DTT, pH 7.4, ionic strength $I = 66$ mM, $[Na^+] = 50$ mM). (*B*) Location of mutated residues in the nucleosome. The region of DNA implicated in binding the lysine-rich region of the NBD is highlighted in red. Color coding as in Fig. 1. (*C*) Gel-shift assay with peptide/DNA ratios of 1, 2, and 5, respectively. LANA is the Kaposi's sarcoma-associated herpivirus latency-associated nuclear antigen peptide (15). The DNA includes 167 bp with the 601 sequence in the middle. (*D* and *E*) Experimental NMR titration data and fits to a cooperative binding model accounting for weak nonspecific binding (model 4 in *SI Text*. (*D*) One-dimensional line shapes of H2B Val45γ2 at indicated molar ratio of nucleosome: HMGN2, experimental data in red, fits in blue. (*E*) Experimental (points) and simulated (solid lines) chemical shift titration curves for selected methyl groups. Dashed gray lines in *D* and *E* show best fits for a noncooperative model with identical parameters for nonspecific binding (model 2, *SI Materials and Methods*).

Ala. Gel-shift experiments confirm that the NBD peptide, $HMGN2_{17–43}$, including these Lys residues, is capable of binding to DNA, whereas a shorter peptide excluding the last three Lys residues is not (Fig. 3*C*). Correspondingly, ITC experiments showed that deletion of the C-terminal 14 residues of H2A has only a marginal effect on the net binding affinity (Fig. 3 *A*–*C* and Table S3), consistent with the observation that there are no significant chemical shift changes for methyl groups in this region (Fig. 2*B*).

**Binding Mechanism Revealed by NMR Line Shape Analysis and Titration.** To further investigate the mechanism by which HMGN2 binds to the nucleosome, we analyzed the NMR titration data. Combined fits of the line shape of Val45γ2 in H2B and chemical shift changes of several methyl groups as a function of titrant concentration are consistent with cooperative binding of two HMGN2 molecules to one nucleosome with additional nonspecific, weak binding to the DNA (Fig. 3 *D* and *E* and Fig. S5). The NMR data was fit to a model where the dissociation constants for the first and second HMGN2 ligands are approximately 1.5 μM and approximately 0.17 μM, respectively, corresponding to a Hill coefficient of 1.4. The lifetime of the fully bound complex is approximately 20 ms (dissociation rate approximately 50 $s^{-1}$), whereas the association rate constant is approximately $3 \cdot 10^8$ $M^{-1}$ $s^{-1}$, which is significantly higher than for diffusion-controlled reactions, indicating that attractive electrostatic forces play an important role in the HMGN2-nucleosome interaction (23) (*SI Materials and Methods*). The ITC data are fully consistent with this binding model (Fig. 3*A* and *SI Materials and Methods*).

## Discussion

Taken together, our data (CSP, PRE, ITC, and gel shift) indicate that the NBD (residues 19–42) binds to the folded core of the nucleosome rather than to the histone tails. The N-terminal Arg-rich (Arg22, Arg23, and Arg26) region of the NBD is associated with the acidic patch of the H2A-H2B dimer, whereas the C-terminal Lys-rich (Lys39, Lys41 and Lys42) portion of the NBD interacts with the DNA near the exit/entry point. With the experimental data as restraints, we docked the NBD to the nucleosome using the HADDOCK program (24) (*SI Materials and Methods* and Fig. S6), showing that the 24 amino acid NBD is well capable of binding to both binding sites simultaneously by adopting an extended conformation (Fig. 4*A*). Overall, the NBD may be described as a "staple" that holds the histone core and nucleosomal DNA together.

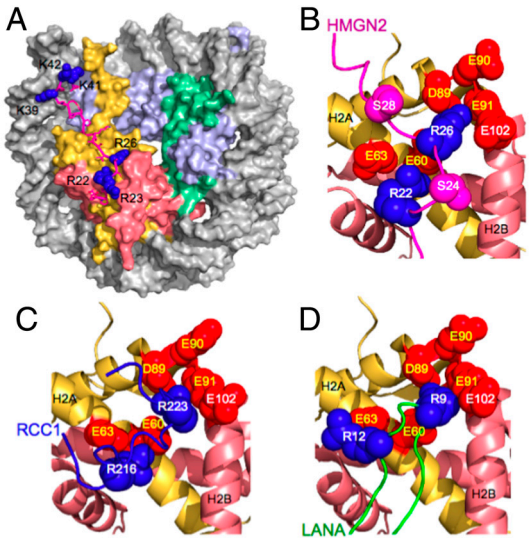


**Fig. 4.** *A docking structure of the NBD-nucleosome complex and comparison of its acidic patch region with those of the RCC1- and LANA-nucleosome complexes.* (*A*) The NBD structure is shown with sticks except that the side chains of the positively charged residues (Arg22, Arg23, Arg26, Lys39, Lys41, and Lys42) are indicated with blue balls. The nucleosome is presented as a surface. *B*, *C*, and *D* display the interactions of the two Arg residues (blue spheres) in HMGN2, RCC1, and LANA with the residues in the acidic patch (red spheres), respectively. Residues Ser24 and Ser28 in the NBD are shown with magenta balls.

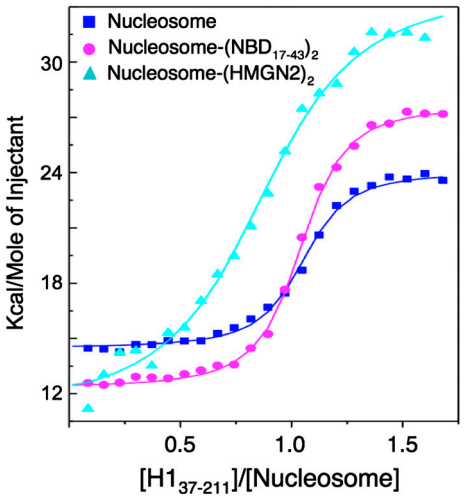


**Fig. 5.** *HMGN2 interferes with the binding of linker histone H1 to the nucleosome as measured by ITC. Drosophila* linker histone $H1_{37–211}$ was titrated into a solution (20 mM Tris-HCl, pH 7.4, 1 mM EDTA and 1 mM DTT) containing free nucleosome (blue square), the nucleosome-$(HMGN2_{1–43})_2$ complex (magenta circle), and the nucleosome-$(HMGN2)_2$ complex (cyan triangle) at 25 °C, with corresponding equilibrium dissociation constants ($K_D$s) of 0.10 μM, 0.10 μM, and 0.57 μM, respectively. The titration results fit to a model in which one H1 molecule binds to one nucleosome. The nucleosome is the same as that used in NMR studies.

The calculated structure of the HMGN2-nucleosome complex shows that most of the residues in the NBD fill the valleys on the surface of the nucleosome (Fig. 4*A* and Fig. S6). The side chains of residues Arg22 and Arg26 in the NBD interact with the carboxyl groups of H2A residues Glu60, Glu63, Asp89, and Glu91 in the acidic patch (Fig. 4*B*). Amino acids 28–38 bridge the acidic patch region and DNA interaction sites and include four Pro residues, which likely play a role in maintaining an extended conformation and reducing the entropic cost upon binding of HMGN2 to the nucleosome. The conserved positively charged Lys residues (Lys39, Lys41, and Lys42) in the C-terminal region of the NBD interact with the phosphates in the minor groove of the DNA at superhelix location +6.5, half a helical turn from the entry/exit point (Fig. 4*A* and Fig. S6).

Interestingly, the acidic patch has also been shown to bind the N-terminal tail of histone H4 (7, 25), the switchback loop of RCC1 (16) (Fig. 4*C*) and Kaposi's sarcoma-associated herpesvirus LANA (latency-associated nuclear antigen) peptide (15) (Fig. 4*D*). Indeed, we found that binding of the LANA peptide to the nucleosome also affects the chemical shifts of methyl groups close to the acidic residues (Fig. S6). The four proteins share no sequence homology but all use two Arg residues for binding. In addition, RCC1 also binds to nucleosomal DNA near the entry/exit point, but using residues in three disjoining regions of its polypeptide chain (16).

Our experimental results clarify several earlier observations. By binding to both core histones and nucleosomal DNA, the NBD would be expected to stabilize the nucleosome. Indeed, nucleosomes bound to either full-length HMGN2 (26) or the NBD (13) are more resistant to thermal denaturation than when in the free state. The staple feature of the NBD suggests that HMGNs may act in opposition to ATP-dependent chromatin remodeling factors by restricting the motion of the DNA in the nucleosome or sterically blocking remodeling factors from binding to the nucleosome (10). Steric interference by HMGNs may also affect the ability of histone modifiers to access and modify their nucleosomal targets (11). The electrostatic nature of the HMGN2-nucleosome interaction explains how HMGN2 can both bind strongly to chromatin, yet be transiently associated with each single site (27).

More importantly, the overall architecture of the HMGN2-nucleosome complex suggests a mechanism for the function of HMGNs, which is independent of the details of the docking structure. The C-terminal region of the NBD binds to nucleosomal DNA near the entry/exit point, placing the long-disordered C-terminal tail of HMGN2 near the linker DNA and the dyad axis so as to interfere with the binding of linker histone H1 to these regions (28). We tested this prediction by examining the effect of HMGN2 and $HMGN2_{1–43}$ on H1 binding to the nucleosome (Fig. 5). We found that HMGN2 increased the equilibrium dissociation constant of H1 by a factor of approximately 6, whereas $HMGN2_{1–43}$ that does not include the C-terminal tail had essentially no effect on H1 binding, indicating that it is the C-terminal tail of HMGN2 that interferes with the binding of H1 (Fig. 6). These results are in line with the observations that HMGNs decrease the compaction of chromatin induced by linker histone H1 in vitro (8) and compete with histone H1 for binding to chromatin in vivo (29). Moreover, our results provide the structural basis for the release of HMGNs from chromatin upon phosphorylation of Ser24 and Ser28 during mitosis (30). As these two residues are very close to the acid patch, the negative charges created by phosphorylation result in unfavorable electrostatic interactions with the acidic patch and subsequent destabilization of the HMGN2-nucleosome complex (Fig. 6). Such a mechanism is likely to play an important role in the regulation of structure

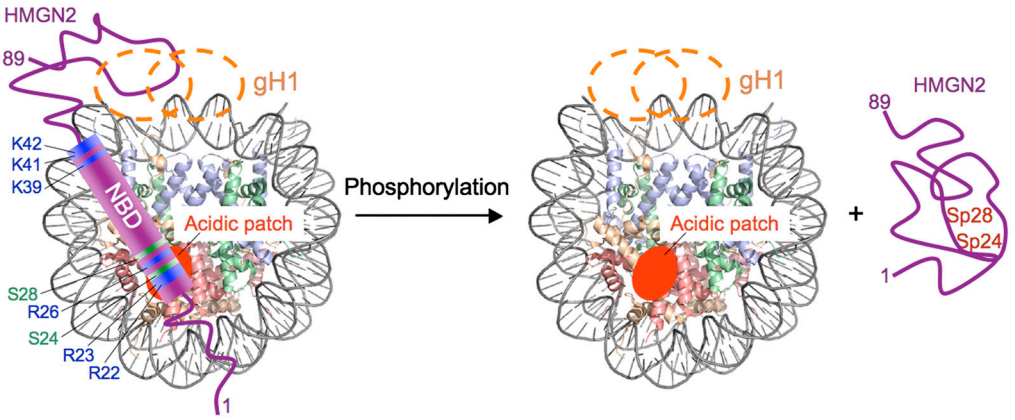


**Fig. 6.** *Implications for the function of HMGNs*. The NBD is shown in cylinder. The disordered terminal regions of HMGN2 are shown in lines. For clarity, only one HMGN2 is shown here (a model with two HMGN2 and one nucleosome is shown in Fig. S6). Earlier studies have shown that regions around the DNA entry/exit point and the dyad of the nucleosome are the approximate binding sites of the globular domain of H1 (gH1, dashed orange oval) (28), which are close to the disordered C-terminal region of HMGN2. Phosphorylation of Ser24 and Ser28 of the NBD induces the dissociation of HMGNs from the nucleosome due to unfavorable electrostatic repulsion with the acidic patch.

and function of chromatin in vivo because HMGN2 is an abundant protein (31).

In summary, we have revealed the architecture of the HMGN2-nucleosome complex by methyl-TROSY NMR combined with mutational analysis, providing key insights into the structural basis of HMGN function. Anchored to the histone core and the nucleosomal DNA as a staple, HMGNs are in a position to interfere with linker histone H1 binding and to promote chromatin decompaction while they can be dissociated from the nucleosome by phosphorylation during mitosis. Finally, with the chemical shifts of methyl groups in the nucleosome now available, the methyl-TROSY approach can be readily used to investigate other important nucleosome-binding interactions including much larger complexes (up to megaDalton size) (18), enhancing our understanding of the dynamic regulation of chromatin structure and function.

## Materials and Methods

**Expression and Purification of Isotope-Labeled Histones and HMGN2.** BL21(DE3) codonplus were transformed with pET21b plasmids encoding histones or HMGN2 and subsequently grown in M9 minimal medium containing desired isotopes at 37 °C. Methyl labeling of Ile-δ1-[$^{13}CH_3$] and Val/Leu-[$^{13}CH_3$, $^{12}CD_3$] (ILV labeling) followed the procedure of Tugarinov et al. (32). Histones and HMGN2 were purified as described before (33, 34). Mutations were made using the QuikChange kit (Stratagene) and verified by DNA sequencing. HMGN2 mutant (A88W) was used to allow convenient concentration measurements. Fragments of HMGN2 including residues 17–36, 17–43, and 1–43 were produced using pGEX-6P-1 GST Expression Vector (GE Healthcare). The resulting GST fusion proteins were purified by GST-Agarose (Sigma), on-column digestion with PreScission Protease (GE Healthcare), and RP-HPLC.

**Purification of 601 DNA and Reconstitution of Nucleosomes.** A high-copy number plasmid containing 12 tandem repeats of a 167 base pair strong positioning DNA sequence (Widom's 601) was transformed to TOP10 cells (Invitrogen) (25). The plasmid was purified according to Dyer et al. (35). The 167-bp fragment was released from the vector by ScaI digestion and purified by PEG fractionation in the presence of 0.5 M sodium chloride. Reconstitution of the nucleosome followed the procedure of ref. 35. The nucleosome was isolated from free DNA at room temperature using a DEAE-5PW ion-exchange HPLC column and, after the elution from the column, the nucleosome was immediately dialyzed.

**NMR Spectroscopy.** Reconstituted nucleosomes with ILV-labeled histones were buffer exchanged into NMR buffer (99% $D_2O$, 20 mM sodium phosphate, pD 6.0 unless noted otherwise). The concentration of NMR samples was typically 100–200 μM in nucleosomes. All NMR experiments were carried out on an 11.7-T (500 MHz $^1H$ frequency) spectrometer equipped with a room-temperature probe head or a 14.1-T (600 MHz) spectrometer with a cryoprobe. Assignment experiments were carried out at 45 °C, whereas the HMGN2 interaction study was done at 35 °C.

Methyl-TROSY spectra were typically recorded with acquisition times $t_1$ and $t_2$ of 30 and 64 ms, respectively. All data were processed using NMRPipe (36) and analyzed with NMRView (37) or Sparky (38).

**Chemical Shift Assignment of Methyl Groups.** Totally, 59 Ile to Leu or Leu/Val to Ile point mutations were made in the histones (Table S1). Comparison of the methyl-TROSY spectra of mutant and wild-type nucleosomes allowed unambiguous assignment of all 28 Ile residues and 40 Leu/Val methyl groups (Fig. S2). A total of six NOESYs with mixing times of 200 ms were obtained on wild-type nucleosomes reconstituted with either ILV-labeled H2B, H3, H4, H2A/H2B, H2A/H3, or H3/H4. The observed pattern of intra- and intermolecular NOEs was carefully compared with the network of short methyl–methyl distances in the crystal structure [2PYO (39)] (Fig. S2). In addition, four NOESYs with 50-ms mixing times were recorded on nucleosomes with Leu/Val-[$^{13}CH_3$, $^{13}CH_3$]-labeled H2A, H2B, H3 or H4, allowing unambiguous pairing of the resonances corresponding to the two methyls within the same Leu or Val residue (Fig. S2). Finally, stereospecific assignments were obtained for several Leu and some Val residues based on distinguishable NOE patterns for the δ1/γ1 and δ2/γ2 methyl groups. Such assignments were accepted only if (*i*) the residue has a rigid side chain orientation, as indicated by low crystallographic B factors and high $S^2$ order parameters and (*ii*) the value of $\chi_2$ predicted on the basis of the observed chemical shift difference $\Delta\delta = \delta^{\delta 1}$-$\delta^{\delta 2}$ (for Leu residues only) corresponds to the observed $\chi_2$ angle in the crystal structure (40). In total, the chemical shifts for 89% of the 170 methyl groups were assigned at a level of 91%, 100%, 93%, and 73% completion for H2A, H2B, H3, and H4, respectively.

**NMR Chemical Shift Perturbation.** Nucleosomes reconstituted with either ILV-labeled H2A, H2B, or H3/H4 were used for a HMGN2 titration experiment monitored by NMR. Both HMGN2 and nucleosome samples were buffer exchanged to 99% $D_2O$, 20 mM sodium phosphate, pD 7.4, ionic strength $I = 49$ mM, and $[Na^+] = 35$ mM. Stock concentrations of HMGN2 were 2.1 mM for the titration with H2B-labeled nucleosomes (160 μM) and 1.0 mM for the titration with H2A (100 μM) and H3/H4 labeled (50 μM) nucleosomes. Methyl-TROSY spectra were measured for the free nucleosome and after each addition of HMGN2 at 35 °C. To identify the binding site of HMGN2, the average, weighted CSP of the histone ILV residues was calculated. For the titration involving H2B-labeled nucleosomes, 17 points were taken in the range of 1:0 and 1:3.3 (nucleosome:HMGN2) molar ratio. The titration data sets with H2A- and H3/H4-labeled nucleosomes comprised 13 and 5 points, respectively. Data from the H2B titration were used to extract binding affinities and dissociation rates as described below.

**Paramagnetic Spin-Labeling Experiments.** The HMGN2 (A88W) spin labels were achieved by introducing a single Cys mutant at the desired position, which was linked to MTS-EDTA-$Mn^{2+}$ (Toronto Research Chemicals). Intermolecular PRE measurements were done at 35 °C at a nucleosome:HMGN2 molar ratio of 1:1.5 to avoid effects from nonspecific binding. To ensure fast exchange between free and bound forms, measurements were done at pD 6.0, where the exchange rate is approximately 1,000–1,500 $s^{-1}$. Peak intensities were quantified in methyl-TROSY spectra of paramagnetic ($Mn^{2+}$) or diamagnetic ($Ca^{2+}$) samples at identical concentrations (approximately 100 μM nucleosome). The uncertainties in peak intensities were estimated from the noise level in the spectra. The resulting ratios were averaged for the two methyls of Leu/Val residues. We note that labeling with (1-oxy-2,2,5,5-tetramethyl-pyrroline-3-$\Delta^3$-methyl)methanethiosulfonate (MTSL) led to results that are difficult to interpret. The same label affected NMR signals of methyl groups at very different locations in the nucleosome. We speculate that MTSL might have caused some nonspecific binding of HMGN2 to the nucleosome.

**Isothermal Titration Calorimetry Experiments.** Calorimetric titration of wild-type or mutant HMGN2 (A88W) to wild-type or mutant nucleosome was performed using a MicroCal VP-ITC titration microcalorimeter at 35 °C. Binding isotherms were generated by plotting the heat change of the binding reaction against the ratio of total concentration of HMGN2 to total concentration of the nucleosome. The heat of binding ($\Delta H$), the stoichiometry of binding ($n$), and the dissociation constant ($K_D$) were determined by fitting the observed binding isotherm to a binding model with either noncooperative or cooperative (specific) binding, in both cases including nonspecific, weak DNA binding (*SI Materials and Methods* and Table S2). In the case of H1 binding, the titration data fits to a model in which one H1 molecule binds to one nucleosome.

**Gel-Shift Assay** HMGN2 peptides corresponding to residues 17–36, 17–43, and LANA peptide corresponding to residues 1–23 were mixed separately with the 167-bp 601-DNA fragment at molar ratios of 1, 2, and 5 in 1× TBE buffer (90 mM Tris/64.6 mM boric acid/2.5 mM EDTA, pH 8.3) for 15 min on ice. The electrophoresis was run using 1.2% agarose gel.

**ACKNOWLEDGMENTS.** We thank Drs. C. Wu, K. Luger, and T. Richmond for plasmids of histones and DNA, C. Klee, C. Wu, and M. Lichten for comments on the manuscript, and A. Bonvin and Y. Postnikov for helpful discussions. This work was supported by the intramural research program of National Cancer Institute (to Y.B.) and grants from the National Sciences and Engineering Research Council of Canada (to L.E.K.) and Canadian Institutes of Health Research (to L.E.K.). L.E.K. holds a Canada Research Chair in Biochemistry. H.K. acknowledges a JSPS fellowship and H.v.I. received support from the Niels Stensen Foundation as well as a Veni-fellowship from the Dutch Science Foundation.

1. Becker PB, Horz W (2002) ATP-dependent nucleosome remodeling. *Annu Rev Biochem* 71:247–273.

2. Nemergut ME, Mizzen CA, Stukenberg T, Allis CD, Macara IG (2001) Chromatin docking and exchange activity enhancement of RCC1 by histones H2A and H2B. *Science* 292:1540–1543.

3. Carroll CW, Silva MC, Godek KM, Jansen LE, Straight AF (2009) Centromere assembly requires the direct recognition of CENP-A nucleosomes by CENP-N. *Nat Cell Biol* 11:896–902.
4. Tan S, Davey CA (2011) Neucleosome structural studies. *Curr Opin Struct Biol* 21:128–136.
5. Kornberg RD, Lorch Y (1999) Twenty-five years of the nucleosome, fundamental particle of the eukaryote chromosome. *Cell* 98:285–294.
6. Khorasanizadeh S (2004) The nucleosome: From genomic organization to genomic regulation. *Cell* 116:259–272.
7. Luger K, Mader AW, Richmond RK, Sargent DF, Richmond TJ (1997) Crystal structure of the nucleosome core particle at 2.8 A resolution. *Nature* 389:251–260.
8. Ding FH, Bustin M, Hansen U (1997) Alleviation of histone H1-mediated transcriptional repression and chromatin compaction by the acidic activation in chromosomal HMG-14. *Mol Cell Biol* 17:5843–5855.
9. Hock R, Furusawa T, Ueda T, Bustin M (2007) HMG chromosomal proteins in development and disease. *Trends Cell Biol* 17:72–79.
10. Rattner BP, Yusufzai T, Kadonaga JT (2009) HMGN proteins act in opposition to ATP-dependent chromatin remodeling factors to restrict nucleosome mobility. *Mol Cell* 34:620–626.
11. Lim JH, et al. (2004) Chromosomal protein HMGN1 modulates histone H3 phosphorylation. *Mol Cell* 15:573–584.
12. Mardian JK, Paton AE, Bunick GJ, Olins DE (1980) Nucleosome cores have two specific binding sites for nonhistone chromosomal proteins HMG 14 and HMG 17. *Science* 209:1534–1536.
13. Crippa MP, Alfonso PJ, Bustin M (1992) Nucleosome core binding region of chromosomal protein HMG-17 acts as an independent functional domain. *J Mol Biol* 228:442–449.
14. Taverna SD, Li H, Ruthenburg AJ, Allis CD, Patel DJ (2007) How chromatin-binding modules interpret histone modifications: Lessons from professional pocket pickers. *Nat Struct Mol Biol* 14:1025–1040.
15. Barbera AJ, et al. (2006) The nucleosomal surface as a docking station for Kaposi's sarcoma herpesvirus LANA. *Science* 311:856–861.
16. Makde RD, England JR, Yennawar HP, Tan S (2010) Structure of RCC1 chromatin factor bound to the nucleosome core particle. *Nature* 467:562–566.
17. Tugarinov V, Hwang JE, Ollerenshaw JE, Kay LE (2003) Cross-correlated relaxation enhanced 1H[bond]13C NMR spectroscopy of methyl groups in very high molecular weight proteins and protein complexes. *J Am Chem Soc* 125:10420–10428.
18. Sprangers R, Kay LE (2007) Quantitative dynamics and binding studies of the 20S proteasome by NMR. *Nature* 445:618–622.
19. Gelis I, et al. (2007) Structural basis for signal sequence recognition by the 204-kDa SecA motor ATPase. *Cell* 131:756–769.
20. Thastrom A, Bingham LM, Widom J (2004) Nucleosomal locations of dominant DNA sequence motifs for histone-DNA interactions and nucleosome positioning. *J Mol Biol* 338:695–709.
21. Clore GM, Tang C, Iwahara J (2007) Elucidating transient macromolecular interactions using paramagnetic relaxation enhancement. *Curr Opin Struct Biol* 17:603–616.
22. Ueda T, Catez F, Gerlitz G, Bustin M (2008) Delineation of the protein module that anchors HMGN proteins to nucleosomes in the chromatin of living cells. *Mol Cell Biol* 28:2872–2883.
23. Alsallaq R, Zhou H-X (2008) Electrostatic rate enhancement and transient complexes of protein-protein association. *Proteins* 71:320–335.
24. Dominguez C, Boelens R, Bonvin AMJJ (2003) HADDOCK: A protein-protein docking approach based on biochemical or biophysical information. *J Am Chem Soc* 125:1731–1737.
25. Dorigo B, et al. (2004) Nucleosome arrays reveal the two-start organization of the chromatin fiber. *Science* 306:1571–1573.
26. Paton AE, Wilkinson-Singley E, Olins DE (1983) Nonhistone nuclear high mobility group proteins 14 and 17 stabilize nucleosome core particles. *J Biol Chem* 258:13221–13229.
27. Phair RD, Misteli T (2000) High mobility of proteins in the mammalian cell nucleus. *Nature* 404:604–609.
28. Thomas JO (1999) Histone H1: Location and role. *Curr Opin Cell Biol* 11:312–317.
29. Catez F, Brown DT, Misteli T, Bustin M (2002) Competition between histone H1 and HMGN proteins for chromatin binding sites. *EMBO Rep* 3:760–766.
30. Prymakowska-Bosak M, et al. (2001) Mitotic phosphorylation prevents the binding of HMGN proteins to chromatin. *Mol Cell Biol* 21:5169–5178.
31. Boumba VA, Seferiadis K, Vougiouklakis T (2004) Content of the HMG-17 chromosomal protein in porcine tissues. *Protein Pept Lett* 11:515–519.
32. Tugarinov V, Kanelis V, Kay LE (2006) Isotope labeling strategies for the study of high-molecular-weight proteins by solution NMR spectroscopy. *Nat Protoc* 1:749–754.
33. Zhou Z, et al. (2008) NMR structure of chaperone Chz1 complexed with histones H2A.Z-H2B. *Nat Struct Mol Biol* 15:868–869.
34. Lim JH, Catez F, Birger Y, Bustin M (2004) Preparation and functional analysis of HMGN proteins. *Methods Enzymol* 375:323–342.
35. Dyer PN, et al. (2004) Reconstitution of nucleosome core particles from recombinant histones and DNA. *Methods Enzymol* 375:23–44.
36. Delaglio F, et al. (1995) NMRPipe: A multidimensional spectral processing system based on UNIX pipes. *J Biomol NMR* 6:277–293.
37. Johnson BA, Blevins RA (1994) NMRView: A computer program for the visualization and analysis of NMR data. *J Biomol NMR* 4:603–614.
38. Goddard TD, Kneller DG SPARKY 3. (University of California, San Francisco), http://www.cgl.ucsf.edu/home/sparky/.
39. Clapier CR, et al. (2008) Structure of the Drosophila nucleosome core particle highlights evolutionary constraints on the H2A-H2B histone dimer. *Proteins* 71:1–7.
40. Mulder FAA (2009) Leucine side-chain conformation and dynamics in proteins from 13C NMR chemcial shifts. *Chembiochem* 10:1477–1479.
41. Ulrich EL, et al. (2007) BioMagResBank. *Nucleic Acids Res* 36:D402–D408.